Bi-Directional *CLLC* Resonant Converter with Integrated Planar Transformer for Energy Storage Systems

Abhinav Soni[1], Student, Ajeet K. Dhakar[2], Member, IEEE
Central Electronics Engineering Research Institute-CSIR, Pilani, India

***Abstract*—This paper presents a bi-directional *CLLC* resonant converter for Energy storage Systems applications, with an integrated planar transformer to enhance power density and curtail the parasitic elements in the transformer. The passive elements in any converter account for the bulkiness, and it can be vanquished by increasing the switching frequency, which can only be entailed by a planar magnetic structure and wide bandgap devices like gallium nitride (GaN) and silicon carbide (Si). Further, FEA analysis is performed to estimate leakage, AC resistance, and core losses for an integrated planar transformer. A simplified voltage/current loop control is implemented on a 32-bit digital signal processor (TMS320F28379D) for battery charging. The advantage of the proposed transformer design is validated through a 300-350 kHz, 500-750 W *CLLC* resonant converter with a peak efficiency of 96.60%**

Keywords*—Isolated bi-directional converter (IBDC), CLLC, Energy storage system (ESS), finite element analysis (FEA), Zero voltage switching (ZVS) and Zero current switching (ZCS)

I. INTRODUCTION

Energy Storage Systems are gaining momentum to be the future's power system. For the commercial/industrial sector, the energy storage system can help alleviate the effect of the utility grid disturbance and can direct power either from the grid to battery pack during peak-off hours or from the battery pack to the grid during peak-on hours. The bi-directional converters are the everlasting key component of an energy storage system due to its ability to condition power from a high-voltage distribution bus (Intermediate 360-400V DC link, or Variable 400-800V DC link, DC Electronic Load) to low-voltage distribution bus (batteries, super-capacitors) and vice versa. The *CLLC* and dual active bridge (DAB) are the two widely adopted DC-DC converter topologies for bi-directional power transfer for an electric vehicle (EV) or an energy storage system (ESS) [1][2][15]. Nonetheless, the soft-switching region for a conventional DAB converter is limited to only narrow output voltage variation [20]. Therefore, the researchers proposed an improved control method for the DAB converter in [17] to improve the conversion efficiency using dual-phase shift (DPS) control. In contrast to DAB, the bi-directional *CLLC* converter can operate with wide output voltage range and soft-switching [2]. Many studies have been carried out over *CLLC* resonant converter. Authors in [2][4] present a design methodology for the *CLLC* converter; these designs make use of wire wound transformer which typically operates at about 50-200 kHz of switching frequency. Nevertheless, none of the aforementioned studies dispense any details on the design and analysis of the high-frequency transformer. To overcome the aforementioned considerations, this paper introduces a detailed design approach and FEA backed analysis for the integrated planar transformer. Also, the PI controller is implemented to achieve constant current (CC) and constant voltage (CV) charging of batteries.

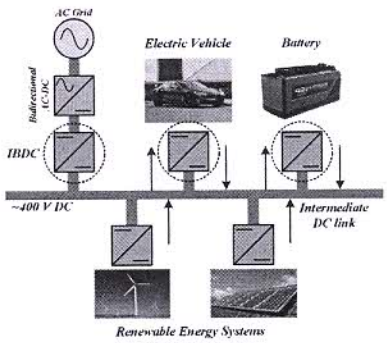

Fig. 1 Typical configuration of LV distribution system using IBDC

The proposed *CLLC* resonant converter for energy storage applications is shown in Fig. 2. The *CLLC* converter has symmetric LLC tank on both primary and secondary sides, resulting in ZVS turn-on of primary side devices and ZCS turn-off of secondary side devices [2][3]. Due to reduced switching loss, the *CLLC* converter is snubber-less [14-17]. The authors in [2][14] present the design methodology and operating modes for *CLLC* resonant converter using fundamental harmonic approximation (FHA). Section II examines the theoretical analysis of the *CLLC* converter, the FHA derived model of *CLLC* converter, forward/reverse modes analysis, and derivations of gain curves. Section III discusses the design methodology for the *CLLC* resonant converter, including the wide input/output voltage range. Section IV presents the design of an integrated planar transformer using PCB stacks for cost optimization. The FEA is performed to estimate the leakage inductance, AC resistance, magnetic flux density, and core losses. Section V presents the hardware experimental results for respective forward and reverse mode of operation; and conversion efficiencies for the same.

II. THEORETICAL ANALYSIS

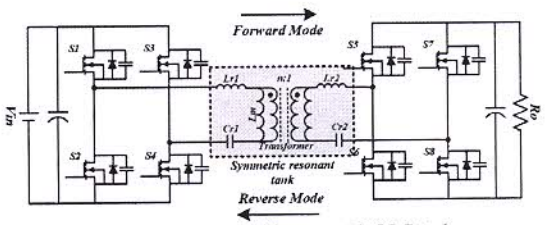

Fig. 2 *CLLC* resonant converter with symmetric LLC tank

Fig. 3 illustrates the waveforms for steady stage operation of the *CLLC* resonant converter operating below the resonant frequency.

A. Operation of CLLC Resonant Converter

Mode I represent a deadtime duration, during which all switches are turned off and no power is transferred to the secondary rectifying stage. The primary resonant current I_{Lr}, charges output capacitance of S_3, S_4 and discharges the output capacitance of S_1, S_2. After this process, the primary current passes through the anti-parallel diode of S_1 and S_2 which makes the switches operate under ZVS.

In II mode S_1, S_2 turns on and power is transferred through the transformer. The I_{Lr} reverses its direction to positive according to S_1, S_2 because the input source forces the current to positive direction through S_1, S_2, the output voltage from the secondary is impressed on the magnetizing inductance L_m, then the magnetizing current I_{Lm} , builds up linearly. Therefore, L_m does not participate in the resonance of the primary stage.

In mode III I_{Lr} equals magnetizing current, at this instant, the power transfer is stopped. Therefore, the secondary current I_s becomes zero, and the output capacitor is not charged by the output current. The I_{Lm} will keep rising till S_1, S_2 are turned off. During this mode, the L_m is no longer clamped by the output voltage. Thus, L_r, C_r and L_m participates in resonance together, and the resonant frequency of this mode is slightly different from other modes.

Mode IV is also a deadtime duration with the switch pair S_3, S_4. The operation is much similar to the mode I; however, the sequence of charging and discharging switches pair is different. The I_{Lr} discharges the output capacitances of S_3, S_4 and charges the output capacitances of S_1, S_2; and S_4, S_5 can turn on with ZVS.

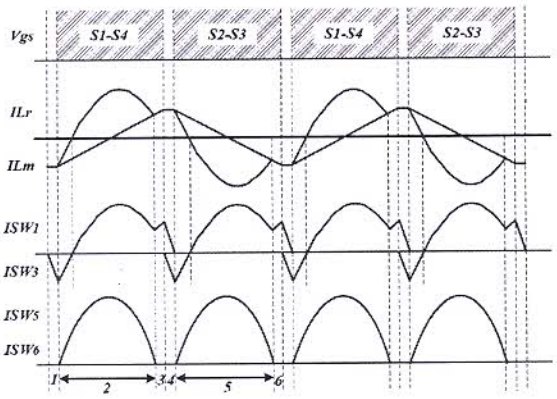

Fig. 3 Operating modes of the *CLLC* resonant converter at below resonance

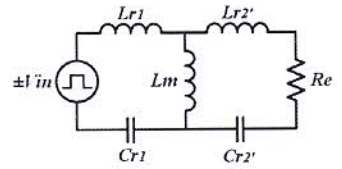

Fig. 4 Equivalent circuit of *CLLC* converter in battery charging mode (BCM)

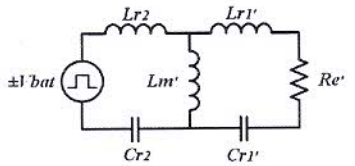

Fig. 5 Equivalent circuit of *CLLC* converter in reverse mode (RM)

In mode V S_3, S_4 turn on and starts transferring power to the secondary side. During this mode, the I_{Lr} changes direction due to the impressed voltage but now in the opposite direction to that in mode II.

After the execution of Mode 5, the resonance and power transfer stops. With no power, the I_s becomes zero and the anti-parallel didoes of output rectifier are softly commutated. A similar operation occurs in the reverse mode, only load, and supply voltage changes.

B. Gain Analysis of CLLC Resonant Converter

i. Equivalent Circuit in the Forward Mode (BCM)

The equivalent circuit of the *CLLC* converter in the forward mode is shown in Fig. 4. Assuming that 'n' is the transformer's turns ratio. Using the FHA, equivalent load resistance R_e can be expressed as follows [2][5].

$$R_e = \frac{8n^2}{\pi^2} R_o \tag{1}$$

Where, R_o is the load resistance in the forward mode. All the equivalent resonant parameters referred to the primary side are as follows.

$$L'_{r2} = n^2 L_{r2}, C'_{r2} = \frac{C_{r2}}{n^2}, \tag{2}$$

The normalized frequency, quality factor, and the resonant frequency is defined as (3)

$$\omega = \frac{\omega_s}{\omega_r}, Q_f = \frac{\sqrt{\frac{L_{r1}}{C_{r1}}}}{R_e}, \omega_r = \frac{1}{\sqrt{L_{r1}C_{r1}}} \tag{3}$$

ii. Equivalent Circuit in the Reverse Mode (RM)

The Equivalent circuit of the *CLLC* converter in reverse mode is shown in Fig. 5, similar to (1) the equivalent load resistance ($R_e{}'$) can be calculated using FHA [2][5][13-14] and is shown in (4)

$$R_e{}' = \frac{8}{n^2\pi^2} R'_o \tag{4}$$

Where, R'_o is the load resistance in reverse mode. Similarly, all the resonant parameters referred to the secondary are as follows.

$$L'_{r1} = \frac{L_{r1}}{n^2}, C_{r1} = n^2 C_{r1}, \omega_r = \frac{1}{\sqrt{L_{r2}C_{r2}}}$$

$$Q_r = \frac{\sqrt{\frac{L_{r2}}{C_{r2}}}}{R_{e'}}, L'_m = \frac{L_m}{n^2} \tag{5}$$

iii. Gain Curves for Forward and Reverse Modes

The general transfer function $H(s)$ can be derived by analyzing Fig. 4 and is expressed in (6)

$$H(s) = \frac{nVout}{Vin} = \frac{R_e(R_2//sL_m)}{R_2(sL_{r1}+\frac{1}{sC_{r1}}+R_2 sL_m)} = \frac{Vin}{\left(\frac{1}{sC_{r1}}+sL_{r1}\right)+\left(n^2 sL_{r2}+\frac{n^2}{sC_{r2}}+\frac{8n^2}{\pi^2}R_o\right)\left[1+\frac{1}{sL_m}\left(\frac{1}{sC_{r1}}+sL_{r1}\right)\right]} \tag{6}$$

Where,

$$R_2 = R_e + sn^2 L_{r2} + \frac{n^2}{sC_{r2}} \tag{7}$$

The gain function of *CLLC* converter in the forward mode is derived in [5], which is expressed as (8)

$$|H(s)|_f = \frac{nV_{out}}{V_{in}} = \frac{1}{\sqrt{\left(\left(\frac{1}{h}-\frac{1}{h\omega^2}+1\right)^2+\left[\frac{1}{\omega}\left(\frac{m}{h}+\frac{1}{hg}+\frac{1}{g}+1\right)Q_f-\omega\left(\frac{m}{h}+m+1\right)Q_f-\frac{Q_f}{hg\omega^3}\right]^2\right)}} \tag{8}$$

Where,

$$h = \frac{Lm}{Lr1}, m = \frac{n^2 Lr2}{Lr1}, g = \frac{Cr2}{n^2 Cr1}$$

Similarly, the gain function for reverse mode can be expressed as in (9)

$$|H(s)|_r = \frac{1}{\sqrt{\left(\left(\frac{1}{p} - \frac{1}{p\omega^2} + 1\right)^2 + \left[\frac{1}{\omega}\left(\frac{r}{p} + \frac{1}{pq} + \frac{1}{q} + 1\right)Q_r - \omega\left(\frac{r}{p} + r + 1\right)Q_r - \frac{Q_r}{pq\omega^3}\right]^2\right)}} \quad (9)$$

Where,

$$p = \frac{Lm}{n^2 Lr2}, r = \frac{Lr1}{n^2 Lr2}, q = \frac{n^2 Cr1}{Cr2}$$

III. Design Methodology

The resonant frequency F_r is selected 300-350 kHz for forward and reverse modes considering the trade-offs between EMI, power density, and efficiency. [12] presents a shielding technique to suppress the common-mode (CM) EMI for an LLC resonant converter employing the planar matrix transformer. Reducing the resonant frequency can help in the reduction of core and copper losses in the transformer but, may cause severe EMI issues [11]. The input voltage range is selected as 360-400V; the converter is aimed to charge low voltage batteries (40-60V) for battery-based energy storage systems; in this view, the turns ratio of transformer T_r is chosen to 7.5. The gain of the converter can be calculated as per the following equation:

$$\frac{V_{out}}{V_{in}} = \frac{G_{forward}}{n} \quad (10)$$

Fig. 6 shows the gain curves for both forward and reverse modes.

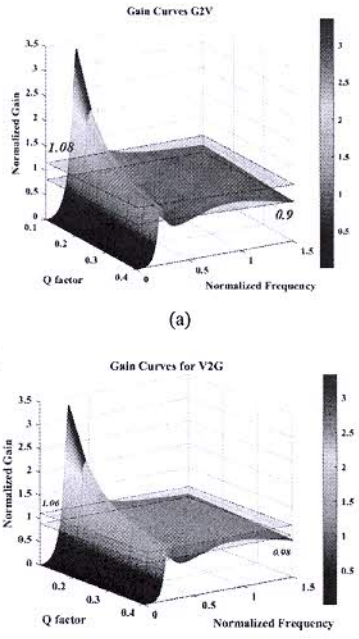

Fig. 6 Gain characteristics of the *CLLC* resonant converter in forward (BCM) and reverse (RM) mode

A. Design of Magnetization Inductance to attain Soft-Switching

ZVS turn-on for high voltage devices and ZCS turn-off for low voltage devices are pivotal to achieve optimal conversion efficiency. The Lm should be designed such as the turn-off current discharges the devices capacitances ($Coss$) within deadtime to achieve soft or ZVS turn-on. In adjunct, operating below the resonant frequency can guarantee the soft commutation of the low voltage devices, because it effectively increases the deadtime duration [2][10][14]. Therefore, the Lm is limited by the maximum switching frequency and is given by (10)

$$Lm \leq \frac{T_{dead}}{16 C_{OSS} F_{rsmax}} \quad (11)$$

Where, F_{rsmax} is the maximum operating frequency, T_{dead} is deadtime; a small Lm guarantees ZVS of high voltage devices at the primary side but small Lm can increase the turn-off losses, and larger Lm causes loss of ZVS; anyhow, both abbreviate the conversion efficiency [2].

B. Resonant Tank Design

Resonant elements must be designed for every possible operating point viz. load changes, frequency changes, circulating energy, and input/output voltage variations [2][10]. The nominal input voltage is kept at 360 V and the nominal load is 4.2 Ω in the forward mode (BCM) and 330 Ω in reverse mode (RM) The turns ratio of the transformer is selected as 7.5:1 considering the 360 V nominal input and 50 V output. The Q factor of the resonant tank is selected as 0.18 ($Q1$) for the forward mode and 0.15 ($Q2$) for reverse mode, delivering 500W of output power. The resonant tanks elements are selected as per the following:

$$C_r = \frac{1}{2\pi Q_1 F_r R_e} \quad (12)$$

$$L_r = \frac{1}{C_r 2\pi {F_r}^2} \quad (13)$$

$$L_m = L_n L_r \quad (14)$$

To reduce the size and weight of the passive elements, the transformer's leakage inductance is utilized as resonant inductors for both sides, which eliminates the additional losses which would have been incurred due to external inductors.

Table IV enlists the key designed parameters for the *CLLC* resonant converter.

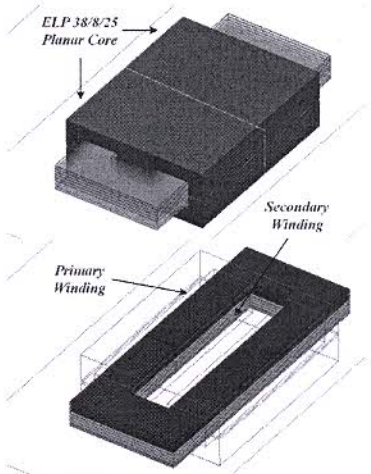

Fig. 7 Construction of the proposed integrated transformer employing two ELP38/8/25 cores and PCB stack windings

IV. Design of Integrated Planar Transformer

To achieve high conversion efficiency, it is desired to mitigate core and winding losses; additionally, to reduce the weight of the converter and increase power density, an integrated planar transformer is proposed and designed. Likewise, 4 PCBs with 2 turns each are used in parallel for the secondary winding. The primary winding is placed on the secondary winding with a layer gap l_b of 0.8 mm, which is utilized to achieve desired leakage inductance and an air gap of 0.7 mm to avoid magnetic flux saturation.

Considering the power requirements and switching frequency, ELP38/8/25 core with 3F4 material from the Ferroxcube is selected. Fig. 7 shows the construction of the transformer, employing two of the ELP38/8/25 core and PCB stacks for the primary and secondary winding. Table I shows the key parameters of the integrated planar transformer.

Table I. Key Parameters of Integrated Planar Transformer

Parameters	Value
Turns ratio Np: Ns	7.5:1
Core Size	ELP 38/8/25 -2
Core material	3F4
Leakage air gap (mm)	0.9
Core air gap (mm)	0.7

With the increase in the number of winding turns, the flux density reduces, resulting in small core loss. Thus, the primary and secondary turns are designed as 15 and 2, respectively. Thus, windings are designed using PCB stacks, each PCB comprises of 4 turns of primary and 4 of these PCBs are used to make primary winding of the transformer, considering the tradeoff between the window area, power rating, and magnetizing inductance. Table II summarizes the PCB stack parameters of the proposed integrated planar transformer.

Table II. PCB Stack Parameters of Integrated Planar Transformer

Parameters	Value
Thickness of Copper on PCB	2Oz
Thickness of one PCB stack	0.8mm
Winding width	4mm
No. of turn per PCB stack (Primary)	4
No. of turn per PCB stack (Secondary)	2

Compared to the Litz wire winding based magnetic structures, PCB winding based magnetics are more sensitive to the high-frequency AC winding loss [12]. The skin effect can have a significant effect on the winding loss at higher frequencies due to increased proximity effect between each turn, making AC resistance significantly high. Considering the 1D model as per [20]

$$F_R = \frac{R_{AC}}{R_{DC}} = M' + \frac{(m^2-1)D'}{3} \quad (15)$$

$$M = \delta h \coth \delta h \quad (16)$$

$$D = 2\delta h \tanh \delta h/2 \quad (17)$$

$$\delta = \sqrt{\frac{j\omega\mu_o\eta}{\rho}} \quad (18)$$

$$\eta = \frac{aN_l}{b} \quad (19)$$

Where, F_R is the ratio of AC winding resistance to the DC winding resistance, M', D' are the real parts of M and D, h is the height of the conductor (which in this case is the thickness of copper in PCB), μ_o is the permeability of free space, a is the width of the conductor, Nl is the number of turns per layer, and b is the window width. Using the above equations, F_R is calculated as 3.579. Thus, the AC resistance of windings can be calculated as:

$$R_{AC} = F_R R_{DC} \quad (20)$$

Table III. Measured and Simulated Parameters of Proposed Integrated Transformer

Parameters	Measured	FEA Simulated
Leakage Inductance Primary	17 μH	16.5 μH
Leakage Inductance Secondary	314 nH	220 nH
AC resistance Primary	627 $m\Omega$	650 $m\Omega$
AC resistance Secondary	10.62 $m\Omega$	11.54 $m\Omega$

Fig. 8 shows the arrangement of the windings and Magnetomotive Force (MMF) for the proposed layout of the integrated planar transformer. Though the MMF across each stack is high compared to the interleaved structures [12], this winding arrangement fulfills the requirement of a resonant inductor. Fig. 9 depicts the completely assembled integrated planar transformer with all PCB stacks and core.

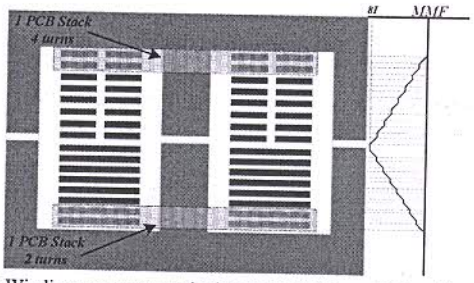

Fig. 8 Winding arrangements in the proposed integrated transformer and the MMF across each stack

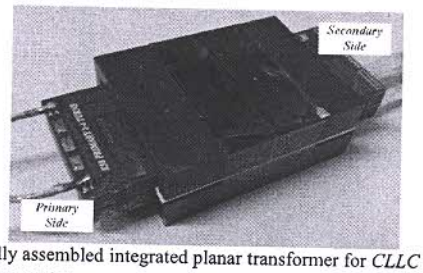

Fig. 9 Fully assembled integrated planar transformer for *CLLC* resonant converter

FEA is carried out to estimate the eddy current loss, hysteresis loss, leakage inductance, AC resistance, magnetic flux density, and winding arrangements. Following equations govern the above-stated parameters, in terms of Maxwell equations:

$$L_{lk} = \frac{1}{I^2}\iiint B.HdV \quad (21)$$

$$I = \iint J.dS \quad (22)$$

$$R_{AC} = \frac{1}{I^2}\iiint \frac{J.J}{\sigma} dV \quad (23)$$

The following equations are presented by authors in [19] and are implemented in Ansys Maxwell software, these equations are calculated via a field calculator tab. A transient 3D FEA is carried out to obtain flux density B, magnetic field strength H, and current density J. Based on these quantities, L_{lk}, B, R_{AC} and core loss density are estimated and shown in Fig. 9

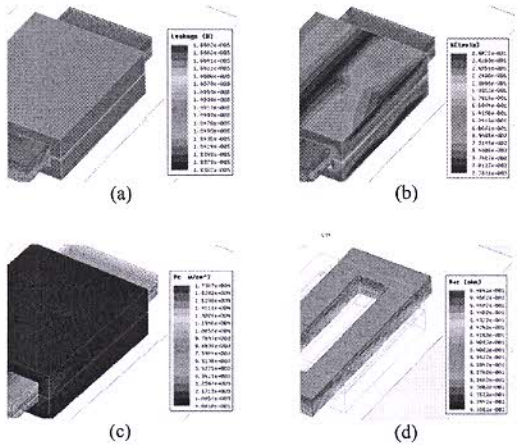

Fig. 9 3D FEA simulation results for (a) leakage inductance, (b) flux density, (c) core loss density and (d) AC resistance of primary winding

V. Experimental Hardware Results

As a verification to the proof of concept, the *CLLC* resonant converter is designed and tested up to 750 W. Photographs of the developed prototype are shown in Fig. 10

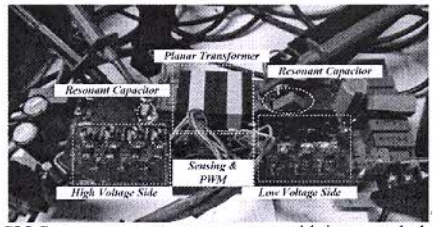

Fig. 10 *CLLC* resonant converter prototype with integrated planar transformer

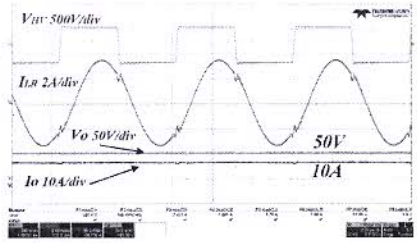

(a)

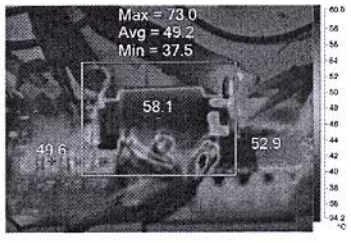

(b)

Fig. 11 (a) Steady state waveforms of *CLLC* resonant converter at 500 W output power, (b) Thermal profile of converter at 500 W

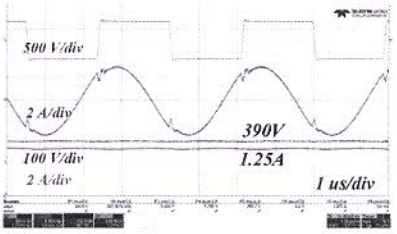

(a)

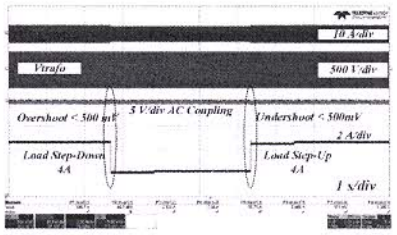

Fig. 12 (a) Reverse mode steady state waveforms at 500 W (b) Voltage loop response; step down from 500 W to 300 W and step up from 300W to 500 W

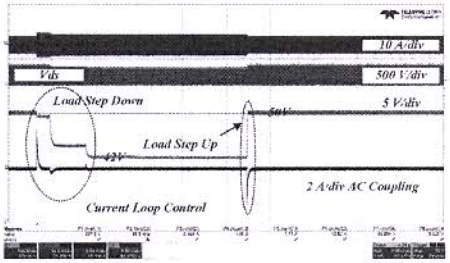

Fig. 13 Waveforms obtained using current loop control for load step down from 450 W to 380 W and 380 W to 450 W

Frequency modulation (FM) is the conventional control for any resonant converter and is widely used for *LLC* and *CLLC* resonant converters. Thus, FM is used to control the control converter in both forward and reverse modes. Fig. 11 (a) shows the steady-state waveforms of the *CLLC* converter operating at 500 W, with 352 kHz of switching frequency and (b) the thermal profile of converter. The output voltage and current are regulated at 50 V and 10 A at an input voltage of 360 V. In need to verify the effectiveness of the voltage and current loops, both step-up and step-down transients are conducted. Fig. 12 (a) shows the reverse mode steady state waveforms (b) shows the closed-loop voltage transients from 500 W to 300 W and 300 W to 500 W respectively. The output voltage is settled at the desired setpoint of 50 V within 50 ms for both the cases.

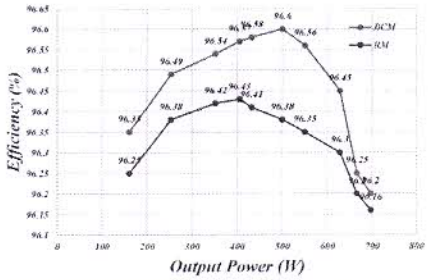

Fig. 14 Conversion efficiency of *CLLC* converter for both BCM and RM modes

Fig. 13 shows the closed-loop current transients from 450 W to 380 W and 380 W to 450W respectively. Synchronous rectification is achieved for low voltage devices using a phase shift technique presented in [20]. Fig. 14 shows the efficiency curves of the *CLLC* converter for BCM and RM modes. Fig. 15 depicts the loss distribution among different elements of the *CLLC* converter.

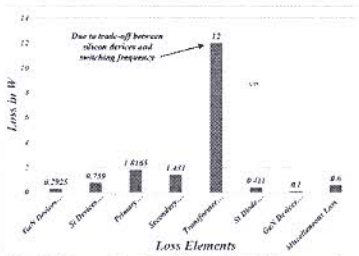

Fig. 15 Loss Distribution of *CLLC* converter

TABLE IV. KEY DESIGNED PARAMETERS FOR *CLLC* RESONANT CONVERTER

Parameters	Forward	Reverse
Resonant frequency F_r (kHz)	350	300
Gain range	0.9-1.08	0.98-1.06
Input Voltage Range (V)	340-380	40-60
Output voltage range (V)	40-60	360-400
Primary resonant capacitor C_{r1}	$11nF$	
Secondary resonant capacitor C_{r2}	$1\mu F$	
Primary resonant inductance L_{r1}	$17\mu H$	
Secondary resonant inductance L_{r2}	$260nH$	
Magnetizing inductance L_m	$120\mu H$	
Switch R_{dson}	$65m\Omega$	
Switch R_{dson}	$2.8m\Omega$	

VI. CONCLUSION

In this paper, a design of a *CLLC* resonant converter with an integrated planar transformer is discussed and FEA simulations are performed to estimate the parameters of a proposed integrated transformer like leakage inductance, AC resistance, flux density, and core loss density. A comparison is performed for the measured and simulated parameters of the same. Furthermore, a high-frequency integrated planar transformer is designed and validated through a GaN-based *CLLC* converter prototype. Ultimately, a closed-loop control is to realize CC/CV charging. Experimental results are presented to validate transformer design and control scheme. The peak efficiencies reach 96.60% at 500 W in BCM mode and 96.43% at 400W in RM mode, respectively.

ACKNOWLEDGMENT

This work has been sponsored by the Science and Engineering Research Board (SERB) for project code GAP-6106 at Central Electronics Engineering Research Institute, which is gratefully acknowledged.

REFERENCES

[1] Chaohui Liu, Jiabin Wang, K. Colombage, C. Gould and B. Sen, "A *CLLC* resonant converter based bidirectional EV charger with maximum efficiency tracking," 8th IET International Conference on Power Electronics, Machines and Drives (PEMD 2016), Glasgow, 2016, pp. 1-6.

[2] J. Jung, H. Kim, M. Ryu and J. Baek, "Design Methodology of Bidirectional *CLLC* Resonant Converter for High-Frequency Isolation of DC Distribution Systems," in IEEE Transactions on Power Electronics, vol. 28, no. 4, pp. 1741-1755, April 2013.

[3] X. Liu et al., "Novel Dual-Phase-Shift Control With Bidirectional Inner Phase Shifts for a Dual-Active-Bridge Converter Having Low Surge Current and Stable Power Control," in IEEE Transactions on Power Electronics, vol. 32, no. 5, pp. 4095-4106, May 2017.

[4] Z. U. Zahid, Z. M. Dalala, R. Chen, B. Chen and J. Lai, "Design of Bidirectional DC–DC Resonant Converter for Vehicle-to-Grid (V2G) Applications," in IEEE Transactions on Transportation Electrification, vol. 1, no. 3, pp. 232-244, Oct. 2015.

[5] Peiwen He and A. Khaligh, "Design of 1 kW bidirectional half-bridge *CLLC* converter for electric vehicle charging systems," 2016 IEEE International Conference on Power Electronics, Drives and Energy Systems (PEDES), Trivandrum, 2016, pp. 1-6.

[6] B. Li, F. C. Lee, Q. Li and Z. Liu, "Bi-directional on-board charger architecture and control for achieving ultra-high efficiency with wide battery voltage range," 2017 IEEE Applied Power Electronics Conference and Exposition (APEC), Tampa, FL, 2017, pp. 3688-3694.

[7] W. Chen, S. Wang, X. Hong, Z. Lu and S. Ye, "Fully soft-switched bidirectional resonant dc-dc converter with a new *CLLC* tank," 2010 Twenty-Fifth Annual IEEE Applied Power Electronics Conference and Exposition (APEC), Palm Springs, CA, 2010, pp. 1238-1242.

[8] H. Kim, M. Ryu, J. Baek and J. Jung, "High-Efficiency Isolated Bidirectional AC–DC Converter for a DC Distribution System," in IEEE Transactions on Power Electronics, vol. 28, no. 4, pp. 1642-1654, April 2013.

[9] S. Zou, J. Lu, A. Mallik and A. Khaligh, "3.3kW *CLLC* converter with synchronous rectification for plug-in electric vehicles," 2017 IEEE Industry Applications Society Annual Meeting, Cincinnati, OH, 2017, pp. 1-6.

[10] J. Deng, S. Li, S. Hu, C. C. Mi and R. Ma, "Design Methodology of LLC Resonant Converters for Electric Vehicle Battery Chargers," in IEEE Transactions on Vehicular Technology, vol. 63, no. 4, pp. 1581-1592, May 2014.

[11] Dianbo Fu, P. Kong, S. Wang, F. C. Lee and Ming Xu, "Analysis and suppression of conducted EMI emissions for front-end LLC resonant DC/DC converters," 2008 IEEE Power Electronics Specialists Conference, Rhodes, 2008, pp. 1144-1150.

[12] B. Li, Q. Li and F. C. Lee, "High-Frequency PCB Winding Transformer With Integrated Inductors for a Bi-Directional Resonant Converter," in IEEE Transactions on Power Electronics, vol. 34, no. 7, pp. 6123-6135, July 2019.

[13] S. Zou, J. Lu, A. Mallik and A. Khaligh, "Bi-Directional *CLLC* Converter With Synchronous Rectification for Plug-In Electric Vehicles," in IEEE Transactions on Industry Applications, vol. 54, no. 2, pp. 998-1005, March-April 2018.

[14] C. Fei, F. C. Lee and Q. Li, "Light load efficiency improvement for high frequency LLC converters with Simplified Optimal Trajectory Control (SOTC)," 2015 IEEE Energy Conversion Congress and Exposition (ECCE), Montreal, QC, 2015, pp. 1653-1659.

[15] W. Chen, P. Rong and Z. Lu, "Snubberless Bidirectional DC–DC Converter With New *CLLC* Resonant Tank Featuring Minimized Switching Loss," in IEEE Transactions on Industrial Electronics, vol. 57, no. 9, pp. 3075-3086, Sept. 2010.

[16] H. Kim, M. Ryu, J. Baek and J. Jung, "High-Efficiency Isolated Bidirectional AC–DC Converter for a DC Distribution System," in IEEE Transactions on Power Electronics, vol. 28, no. 4, pp. 1642-1654, April 2013

[17] H. Bai and C. Mi, "Eliminate Reactive Power and Increase System Efficiency of Isolated Bidirectional Dual-Active-Bridge DC–DC Converters Using Novel Dual-Phase-Shift Control," in IEEE Transactions on Power Electronics, vol. 23, no. 6, pp. 2905-2914, Nov. 2008, doi: 10.1109/TPEL.2008.2005103.

[18] P. L. Dowell, "Effects of eddy currents in transformer windings," in Proceedings of the Institution of Electrical Engineers, vol. 113, no. 8, pp. 1387-1394, August 1966, doi: 10.1049/piee.1966.0236.

[19] D. Reusch, F. C. Lee, Ming Xu and D. Sterk, "Improved transformer design for high frequency VRM applications," 2008 Twenty-Third Annual IEEE Applied Power Electronics Conference and Exposition, Austin, TX, 2008, pp. 1483-1489, doi: 10.1109/APEC.2008.4522920.

[20] Y. Gao, K. Sun, X. Lin and Z. Guo, "A phase-shift-based synchronous rectification scheme for bi-directional high-step-down *CLLC* resonant converters," 2018 IEEE Applied Power Electronics Conference and Exposition (APEC), San Antonio, TX, 2018, pp. 1571-1576, doi: 10.1109/APEC.2018.8341226